Supplemental Document

Optics Letters

Nonlinear terahertz Kerr effect in quasi-2D $MnPS_3$: supplement

LONG CHENG,[1,†] FABIO FORMISANO,[2,†] KIRILL A. GRISHUNIN,[2] SERGEY D. GORELOV,[3] PAUL H. M. VAN LOOSDRECHT,[4] JIAN YAN,[5] XUAN LUO,[5,6] ZHIGAO SHENG,[1,7] AND EVGENY A. MASHKOVICH[4,*]

[1]*Anhui Key Laboratory of Condensed Matter Physics at Extreme Conditions, High Magnetic Field Laboratory, Chinese Academy of Sciences, Hefei 230031, China*
[2]*Radboud University, Institute for Molecules and Materials, Nijmegen 6525 AJ, The Netherlands*
[3]*University of Nizhny Novgorod, Nizhny Novgorod 603022, Russia*
[4]*University of Cologne, Institute of Physics II, Cologne D-50937, Germany*
[5]*Key Laboratory of Materials Physics, Institute of Solid State Physics, HFIPS, Chinese Academy of Sciences, Hefei 230031, China*
[6]*e-mail: xluo@issp.ac.cn*
[7]*e-mail: zhigaosheng@hmfl.ac.cn*
[*]*Corresponding author: mashkovich@ph2.uni-koeln.de*
[†]*These two authors contribute equally to this Letter.*

Supplement DOI: https://doi.org/10.6084/m9.figshare.20338545

Parent Article DOI: https://doi.org/10.1364/OL.457627

Nonlinear terahertz Kerr effect in quasi-2D $MnPS_3$: supplemental document

1. Supplementary Figures

Figure S1. Morphology and crystallographic axes of the sample

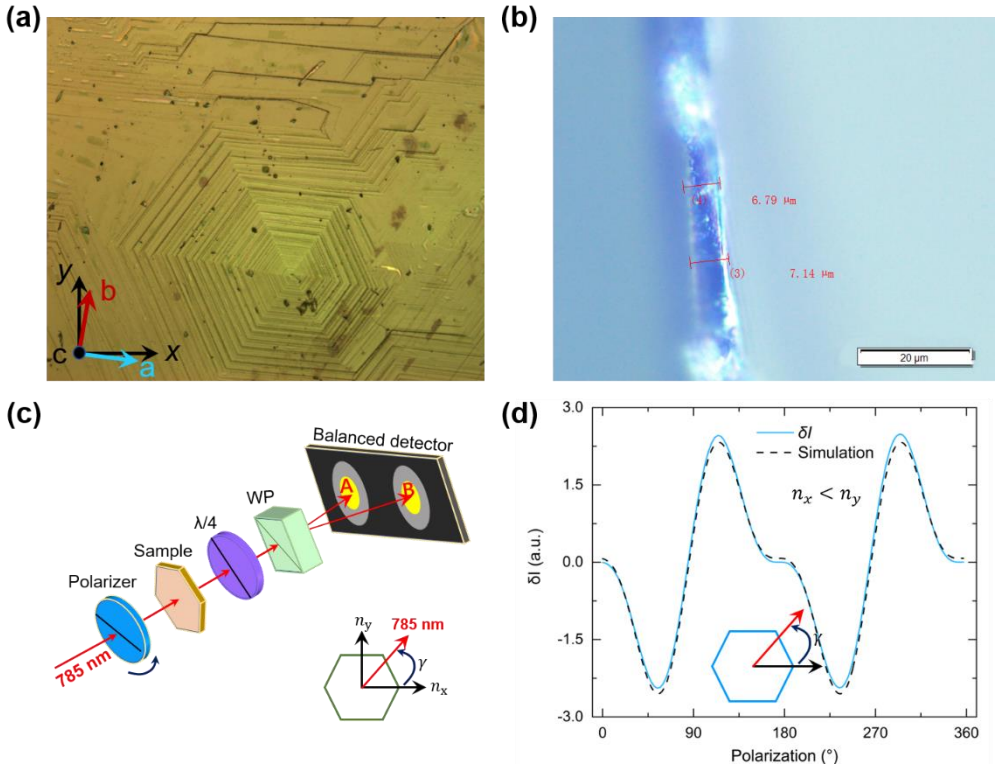

Fig. S1. Morphology of the $MnPS_3$ sample. (a) The amplified surface topography of the crystal. The sample is mounted with *a*-axis deflected by ~10° to the laboratory *x*-axis on the sample plate. (b) Thickness of the sample scaled and marked with microscope. (c) Optical setup used to identify the optical axis. The inset illustrates the configuration of the sample with reference of the hexagonal morphology shown on panel (a). Corresponding output of the balance detector could be expressed as $\delta I_{A-B} \propto -\sin(2\gamma)\ (\cos(\gamma)^2 - 1)\sin[\eta(n_y - n_x)]$, where η is the constant phase shift coefficient. (d) Polarization dependent output of (c), as plotted with solid blue line. The dashed line is simulation result. Consequently, according to the dielectric constant reported before,[1] the *a*- and *b*-axes could be determined and shown in (a) with blue and red arrows, respectively.

Figure S2. THz field strength dependence

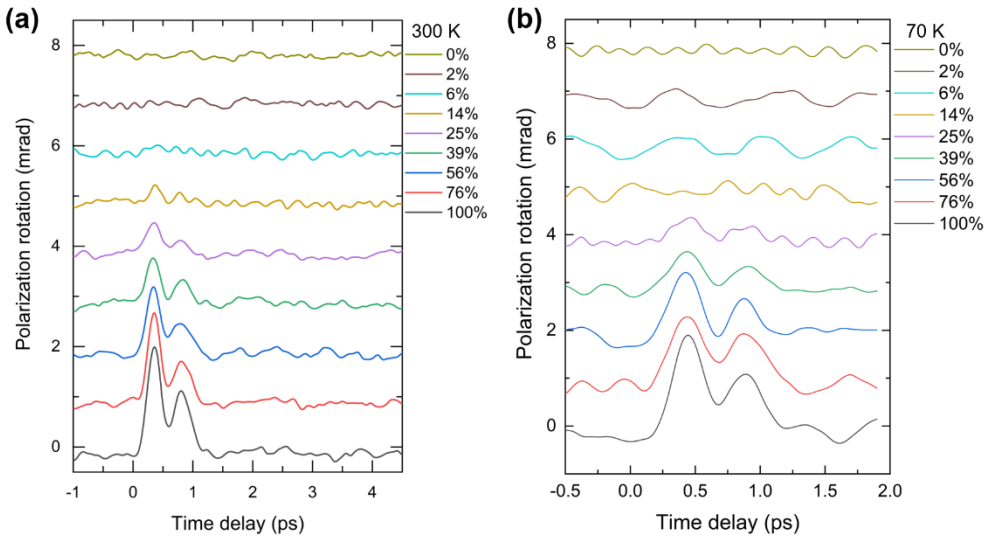

Fig. S2. THz induced probe polarization rotation at different THz pump amplitudes. Panels (a) and (b) demonstrate the results at temperatures of 300 K and 70 K, respectively. The percentages of the incident THz pulse electric field amplitude are shown in the legends, where 100% corresponds to 750 kV/cm.

Figure S3. Schematic of the experimental setup

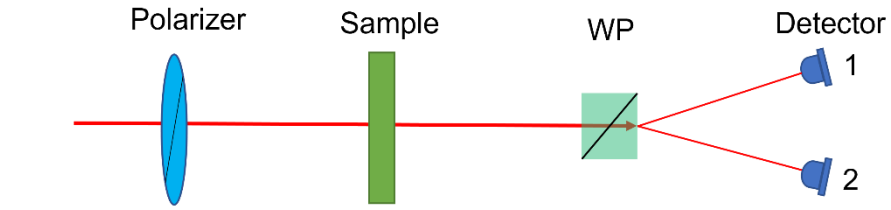

$\pi/4$ $\quad \begin{bmatrix}1\\1\end{bmatrix} \quad \begin{bmatrix}e^{-i\Delta\varphi} & 0\\0 & 1\end{bmatrix} \quad \frac{I_1 - I_2}{I_1 + I_2} = 0$

$\pi/4$ $\quad \begin{bmatrix}1\\1\end{bmatrix} \quad rot \begin{bmatrix}e^{-i\Delta\varphi} & 0\\0 & 1\end{bmatrix} rot' \quad \frac{I_1 - I_2}{I_1 + I_2} \propto -sin4\theta \cdot (\frac{\Delta\varphi}{2})^2$

$$rot = \begin{bmatrix}\cos\theta & \sin\theta\\-\sin\theta & \cos\theta\end{bmatrix} \qquad \Delta\varphi = (n_o - n_e)\frac{2\pi}{\lambda}t$$

Fig. S3. Configuration and corresponding Jones calculus of the experimental setup. Among them, θ is the deflection angle of the incident probe light with respect to its initial polarization state. $\Delta\varphi$ is the phase retardation originating from the refractive index difference $(n_o - n_e)$ of orthogonally polarized probe light components. λ and t denote the wavelength of probe light and thickness of the sample, respectively.

Figure S4. Static relative probe polarization rotation

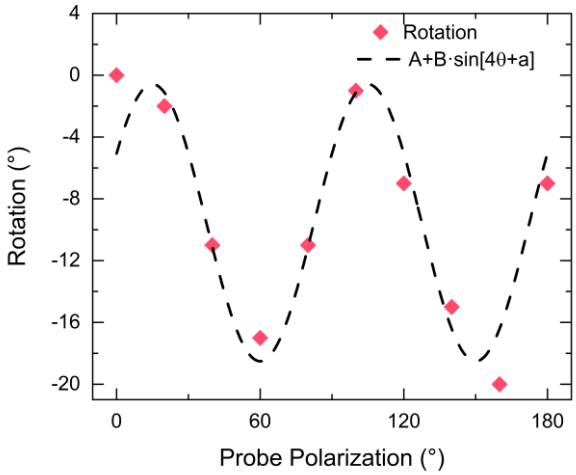

Fig. S4. The static relative probe polarization rotation with THz pump pulse blocked. For the case of performing the measurement of probe polarization dependence, the initial signal of setup should be first balanced when there is no pump field applied on the sample. Afterwards, while balancing the single of the detector at each polarization angle, in addition to the rotation angle synchronized with the probe polarization, an extra angle needs to be further rotated to make the initial signal as zero. This extra angle attributes to the static optical properties of the sample. Here, the probe polarization dependence of the extra angle is plotted and fitted with sinusoidal function (dashed line). Apparently, it shows the symmetry of $\pi/2$ revealing strong anisotropy of $MnPS_3$ (~20° rotation for ~7 μm thick sample).

Figure S5. THz induced ellipticity changes measured at different THz polarizations

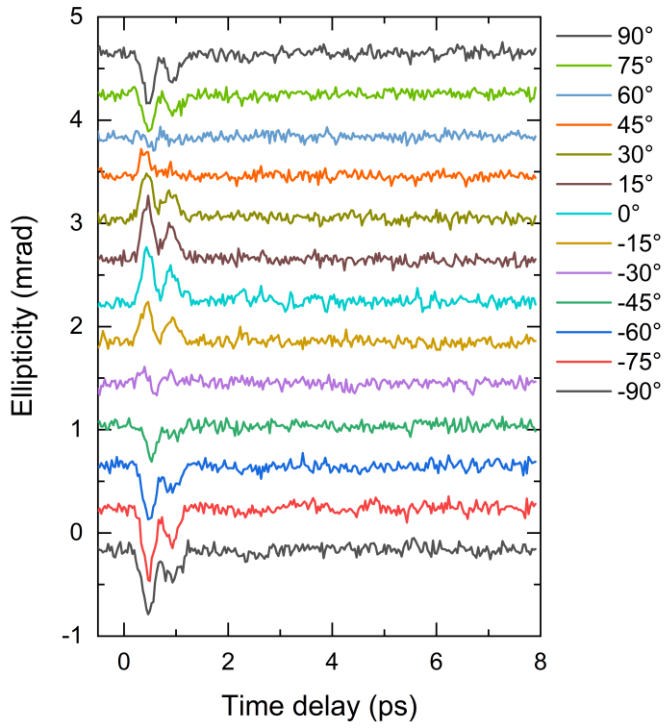

Fig. S5. THz induced probe polarization ellipticity at several THz pump polarization angles β. The THz polarization angles are counted from y-axis with the same step of 15°. An additional quarter-wave plate was installed before WP in Fig. 1(b).

Figure S6. Refractive index of $MnPS_3$ in the THz frequency range

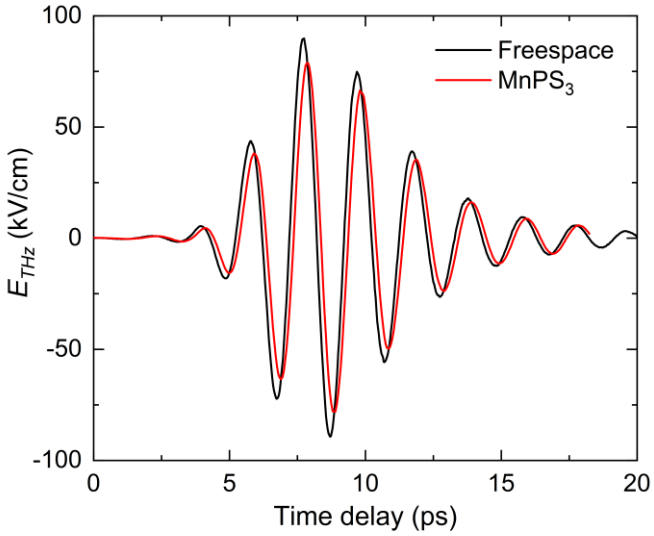

Fig. S6. Refractive index of $MnPS_3$ single crystal in the THz frequency range measured by conventional THz time-domain-spectrometer. The black and red curves are THz waveforms measured after passing through free space and the sample. Following standard Fourier analysis[2], the refractive index $n_{\mathrm{THz}} \approx 1.27$ and extinction coefficient $\kappa_{\mathrm{THz}} \approx 0.64$ of the $MnPS_3$ crystal can be calculated.

2. Supplementary Algorithms

Algorithm S1. Refractive index ellipsoid under the action of THz pulse

According to the theory of EO effect, the electric polarization field (**P**) depends on the external electrical field (**E**) and could be expressed as:

$$\mathbf{P} = \varepsilon_0 \chi_{ij}^{(1)} : \mathbf{E} + \varepsilon_0 \chi_{ijk}^{(2)} : \mathbf{EE} + \varepsilon_0 \chi_{ijkl}^{(3)} : \mathbf{EEE} + \cdots, \tag{S1}$$

in which, ε_0 is the vacuum permittivity and $\chi^{(n)}$ is the *n*-th order component of the electric susceptibility of the sample. While the electrical field ($\mathbf{E} = \mathbf{E}^{(\mathrm{THz})} + \mathbf{E}^{(\mathrm{probe})}$) include components of intense pump light $\mathbf{E}^{(\mathrm{THz})}$ and moderate probe light $\mathbf{E}^{(\mathrm{probe})}$. Afterwards, by expanding the expression and only retaining items related to the EO effect, it could be simplified and written as:

$$P_i = \varepsilon_0 \left(\chi_{ij}^{(1)} E_j + \chi_{ijk}^{(2)} E_j E_k + \chi_{ijkl}^{(3)} E_j E_k E_l \right) + \cdots, \tag{S2}$$

where E_j ($j = 1,2,3$) is the probe pulse electric field components, whilst E_k and E_l are the THz pump electric field components. $MnPS_3$ belongs to the point group of *C2/m*, which includes symmetry operators:

$$\sigma^1 = \begin{bmatrix} -1 & 0 & 0 \\ 0 & -1 & 0 \\ 0 & 0 & -1 \end{bmatrix} \text{ and } \sigma^2 = \begin{bmatrix} -1 & 0 & 0 \\ 0 & 1 & 0 \\ 0 & 0 & -1 \end{bmatrix} \tag{S3}$$

The form of σ^1 (inversion center) implies that the 3-rd order polar tensor $\chi_{ijk}^{(2)}$ would be zero, which means that the Pockels effect is forbidden. This is also in consistent with our experimental result on THz electric field strength dependence, as shown in Fig. 1(d). Consequently, the polarization field could be further simplified as:

$$P_i = \varepsilon_0 \left(\chi_{ij}^{(1)} + 3\chi_{ijkl}^{(3)} E_k^{(\mathrm{THz})} E_l^{(\mathrm{THz})} \right) E_j^{(\mathrm{probe})} \tag{S4}$$

Here $\chi_{ij}^{(1)}$ contributes to the static probe polarization rotation with the THz pulse blocked, corresponding results are shown in the Supplementary Fig. S4. For the sample thickness of ~7 μm, the relative polarization rotation reaches the maximum of ~20°. While $\chi_{ijkl}^{(3)}$ determines the ultrafast Kerr-type EO effect. For simplicity in the subsequent derivations, according to $\varepsilon_{ij} = \varepsilon_0(1 + \chi_{ij}) = \varepsilon_0 + \varepsilon_{ij}^{(1)} + \varepsilon_{ij}^{(3)} + \cdots$, the electric susceptibility tensor could be substituted with dielectric permittivity tensor, which possesses the same symmetry properties. Combining with the symmetry operators of the crystal group ($C2/\mathrm{m}$) and the divergence of Poynting's theorem (conservation of electromagnetic field energy),[3] the 2nd-order tensor could be expressed as:

$$\varepsilon_{ij}^{(1)} = \begin{bmatrix} \varepsilon_{11} & 0 & \varepsilon_{13} \\ 0 & \varepsilon_{22} & 0 \\ \varepsilon_{13} & 0 & \varepsilon_{33} \end{bmatrix} \tag{S5}$$

While for the 4th-order tensor (ε_{ijkl}), by considering symmetry operators of σ^1 and σ^2, these tensor components it contained will also be zero when the indices *2* appears odd times. Which means that *ijk*2(32), *i*222(8) would be zero, in which the *ijk*2 and *i*222 are indices of permittivity

tensor and numbers in parentheses are their amount. Then consider the second law of thermodynamic, $dG = -Sd\theta + dW$, the indices of *ij*, *kl*, and (*ij*)(*kl*) are interchangeable, respectively. As a result, the 4th order dielectric permittivity tensor could be written as a 6×6 matrix:

$$\varepsilon_{mn}^{(3)} = \begin{bmatrix} s_{11} & s_{12} & s_{13} & 0 & s_{15} & 0 \\ s_{12} & s_{22} & s_{23} & 0 & s_{25} & 0 \\ s_{13} & s_{22} & s_{33} & 0 & s_{35} & 0 \\ 0 & 0 & 0 & s_{44} & 0 & s_{46} \\ s_{15} & s_{25} & s_{35} & 0 & s_{55} & 0 \\ 0 & 0 & 0 & s_{46} & 0 & s_{66} \end{bmatrix} \tag{S6}$$

To be note, in the matrix, $s_{mn} = 2s_{ijkl}$, if either *m* or *n*=4, 5, or 6; whilst $s_{mn} = 4s_{ijkl}$, if both *m* and *n* = 4, 5, or 6. Afterwards, for the nonlinear case, the external electrical field of pump pulse normally incident alone the *c*-axis could be expressed as:

$$E_k E_l = \begin{bmatrix} E_1^2 \\ E_2^2 \\ E_3^2 \\ 2E_2E_3 \\ 2E_1E_3 \\ 2E_1E_2 \end{bmatrix} = \begin{bmatrix} E_1^2 \\ E_2^2 \\ 0 \\ 0 \\ 0 \\ 2E_1E_2 \end{bmatrix} \tag{S7}$$

Then, the dielectric permittivity tensor under the interaction of pump pulse could be further expressed as:

$$\varepsilon_{ij}^{(3)} = \begin{bmatrix} s_{11} & s_{12} & s_{13} & 0 & s_{15} & 0 \\ s_{12} & s_{22} & s_{23} & 0 & s_{25} & 0 \\ s_{13} & s_{22} & s_{33} & 0 & s_{35} & 0 \\ 0 & 0 & 0 & s_{44} & 0 & s_{46} \\ s_{15} & s_{25} & s_{35} & 0 & s_{55} & 0 \\ 0 & 0 & 0 & s_{46} & 0 & s_{66} \end{bmatrix} \begin{bmatrix} E_1^2 \\ E_2^2 \\ 0 \\ 0 \\ 0 \\ 2E_1E_2 \end{bmatrix} \tag{S8}$$

Consequently, combining the $\varepsilon_{ij}^{(1)}$ and $\varepsilon_{ij}^{(3)}$, the equation of the refraction index ellipsoid in the presence of electrical field of external pump pulse can be written as:

$$\begin{aligned} x^2\left(\frac{1}{n_1^2} + s_{11}E_1^2 + s_{12}E_2^2\right) + y^2\left(\frac{1}{n_2^2} + s_{12}E_1^2 + s_{22}E_2^2\right) + z^2\left(\frac{1}{n_1^2} + s_{13}E_1^2 + s_{23}E_2^2\right) \\ +2yz\left(2s_{46}E_1E_2\right) + 2xz\left(s_{15}E_1^2 + s_{25}E_2^2\right) + 2xy\left(2s_{66}E_1E_2\right) = 1 \end{aligned} \tag{S9}$$

where n_i $(i = 1,2,3)$ are components of the refractive indexes corresponding to the static $(\varepsilon_{ij}^{(1)})$ optical responses. For the experimental setup, the vector of normally incident electric field with polarization angle of β is:

$$\mathbf{E}^{(\mathrm{THz})}=\begin{bmatrix}E_1\\E_2\\E_3\end{bmatrix}=\begin{bmatrix}E_{\mathrm{THz}}\cos(\beta)\\E_{\mathrm{THz}}\sin(\beta)\\0\end{bmatrix} \tag{S10}$$

where the E_{THz} is amplitude of THz electric field. Then the index ellipsoid could be further expanded as:

$$\begin{aligned}&\left(\frac{1}{n_1^2}+s_{11}E_{\mathrm{THz}}^2\cos(\beta)^2+s_{12}E_{\mathrm{THz}}^2\sin(\beta)^2\right)x^2\\&+\left(\frac{1}{n_2^2}+s_{12}E_{\mathrm{THz}}^2\cos(\beta)^2+s_{22}E_{\mathrm{THz}}^2\sin(\beta)^2\right)y^2\\&+\left(\frac{1}{n_3^2}+E_{\mathrm{THz}}^2s_{13}\cos(\beta)^2+E_{\mathrm{THz}}^2s_{23}\sin(\beta)^2\right)z^2\\&+2xz\left(s_{15}E_{\mathrm{THz}}^2\cos(\beta)^2+s_{25}E_{\mathrm{THz}}^2\sin(\beta)^2\right)+\\&4E_{\mathrm{THz}}^2s_{66}xy\cos(\beta)\sin(\beta)+4E_{\mathrm{THz}}^2s_{46}yz\cos(\beta)\sin(\beta)=1.\end{aligned} \tag{S11}$$

Afterward, since the probe pulse is also normally incident alone *c*-axis of the sample, the index elliptical cross section perpendicular to the propagation direction could be simplified as:

$$\begin{aligned}&\left(\frac{1}{n_1^2}+s_{11}E_{\mathrm{THz}}^2\cos(\beta)^2+s_{12}E_{\mathrm{THz}}^2\sin(\beta)^2\right)x^2+\\&\left(\frac{1}{n_2^2}+E_{\mathrm{THz}}^2s_{12}\cos(\beta)^2+E_{\mathrm{THz}}^2s_{22}\sin(\beta)^2\right)y^2+\\&4E_{\mathrm{THz}}^2s_{66}xy\cos(\beta)\sin(\beta)=1\end{aligned} \tag{S12}$$

Algorithm S2. THz polarization dependence of Kerr EO effect

Based on the expression above, the ellipse of the refraction index is simulated. According to the expression and the simulation result above, one can conclude that the effect of external pump field on the index elliptical section is the variation of rotation angle (ψ) and principle axes ($2n_o$, $2n_e$) of index ellipse. These parameters could be extracted from the elliptical expression and written as:

$$n_o=\left\{\frac{1}{n_1^2}+\frac{E_{\mathrm{THz}}^2}{2}\left[s_{11}+s_{12}+\left(s_{11}-s_{12}\right)\cos(2\beta)\right]\right\}^{-1/2} \tag{S13}$$

$$n_e=\left\{\frac{1}{n_2^2}+\frac{E_{\mathrm{THz}}^2}{2}\left[s_{22}+s_{12}+\left(s_{12}-s_{22}\right)\cos(2\beta)\right]\right\}^{-1/2} \tag{S14}$$

$$\psi=\frac{1}{2}\mathrm{atan}\left\{\frac{4E_{\mathrm{THz}}^2s_{66}\sin(2\beta)}{\frac{1}{n_1^2}-\frac{1}{n_2^2}+\frac{E_0^2}{2}\left[s_{11}-s_{22}+\left(s_{11}+s_{22}-2s_{12}\right)\cos(2\beta)\right]}\right\} \tag{S15}$$

By transforming these expressions into Taylor's series, these parameters above could be simplified as:

$$n_o = n_1 - \frac{n_1^3 E_{\mathrm{THz}}^2 \left[s_{11} + s_{12} + \left(s_{11} - s_{12} \right) \cos(2\beta) \right]}{4} + \cdots \tag{S16}$$

$$n_e = n_2 - \frac{n_2^3 E_{\mathrm{THz}}{}^2 \left[s_{12} + s_{22} + \left(s_{12} - s_{22} \right) \cos(2\beta) \right]}{4} + \cdots \tag{S17}$$

$$\psi = -\frac{2 E_{\mathrm{THz}}{}^2 n_1^2 n_2^2 s_{66} \sin(2\beta)}{n_1^2 - n_2^2} + \cdots \tag{S18}$$

Then, difference of the refraction index of ordinary and extra-ordinary waves will be:

$$\begin{aligned} \Delta n &= n_o - n_e = \Delta n_{\mathrm{static}} + \Delta n_{\mathrm{THz}} \\ &= n_1 - n_2 + E_{\mathrm{THz}}^2 \left\{ \begin{array}{l} \dfrac{n_2^3 \left(s_{12} + s_{22} \right)}{4} - \dfrac{n_1^3 \left(s_{11} + s_{12} \right)}{4} - \\ \cos(2\beta) \left[\dfrac{n_1^3 \left(s_{11} - s_{12} \right)}{4} - \dfrac{n_2^3 \left(s_{12} - s_{22} \right)}{4} \right] \end{array} \right\} + \cdots \\ &= n_1 - n_2 + E_{\mathrm{THz}}{}^2 \{ M - N \cdot \cos(2\beta) \} + \cdots, \end{aligned} \tag{S19}$$

where $\Delta n_{\mathrm{static}}$ and Δn_{THz} are static and THz pulse induced refractive differences, respectively. Consequently, during rotating the azimuth of pump polarization, the variation of the index ellipse possesses the period of π. Then for a certain polarized probe pulse that employed to detect the pump polarization dependent variation of refractive index ellipse, it shows the same period of π, which is in good consistent with our pump polarization dependent results shown in Fig. 2(c).

Algorithm S3. Probe polarization dependence of Kerr EO effect

Besides, for the case of probe polarization dependence measured with the rotation configuration, the symmetry of its optical response depends on if the pump pulse induced extinction coefficient (κ) is taken into account. Specifically, when the sample is pumped with THz pulse, as shown in Fig. 3, only distinct linear birefringence effect (Kerr EO effect) that attributes to the real part of the refraction index is observed. While the variation of the imaginary part of the refraction index is neglectable. Besides, under a certain THz pump excitation, consequent refractive index ellipse is constant. Its symmetry could be distinguished by the probe polarization dependence with the rotation measurement configuration. As shown in the Fig. S3, θ is the azimuth of probe pulse relative to the angle bisector of optical principle axes and $\Delta\varphi$ is the phase shift of ordinary and extra-ordinary probe pulses. Accordingly, combining the Jones matrix of these optical components, it's easy to deduce the output of the balanced detector as:

$$\alpha_K \approx \frac{\left(I_1 - I_2\right)}{2\left(I_1 + I_2\right)} = \frac{1}{2}\sin(4\theta)\sin\left(\frac{\Delta\varphi}{2}\right)^2 \propto \frac{1}{8}\sin(4\theta)\cdot\Delta n^2\cdot\left(\frac{\omega}{c}t\right)^2, \tag{S20}$$

where θ is the rotation angle, I_1, I_2 are intensity of the balanced detector, ω is the frequency of the probe light, c is the speed of light in vacuum and t is the thickness of the sample. Among this formula, the Δn^2could be expanded as:

$$\Delta n^2 = \left(\Delta n_{\text{static}} + \Delta n_{\text{THz}}\right)^2 = \Delta n_{\text{static}}^2 + 2\cdot\Delta n_{\text{static}}\cdot\Delta n_{\text{THz}} + \Delta n_{\text{THz}}^2 \tag{S21}$$

in which the first item responsible for the static optical response and last two contribute to the dynamic Kerr effect induced by THz pulse. Particularly, $\Delta n_{\text{static}}^2$ has been suppressed during the balancing process before the measurement and Δn_{THz}^2 corresponds to a higher order case ($E_0{}^4$), which is negligible. Therefore, only the second term of S21 plays dominant role on the ultrafast Kerr responses. From the expression of the output, the period of the probe polarization dependence is $\pi/2$. In addition, for the case of pump pulse isn't applied on the sample, the optical response is derived from the refractive index ellipse corresponding to the static dielectric permittivity tensor, whose symmetry also shows the period of $\pi/2$, as shown in the supplementary Fig. S3. Both the static and dynamic optical responses are in good consistent with the symmetry of the sample.

Beyond that, by constructing ellipsometry configuration with quarter wave-plate inserted between sample and Wollaston prism, the probe polarization dependence of the Kerr EO effect could be directly characterized. Consequently, the probe polarization dependence of the ellipticity (ϵ_K) could be expressed as:

$$\epsilon_{\text{K}} = \frac{1}{2}\sin(2\theta)\sin(\Delta\varphi) \tag{S22}$$

where only Δn_{THz} is involved in the transient result and from which corresponding Kerr EO coefficient n_{NL} could be calculated directly. Apart from that, the ϵ_{K} would reach the maximum when probe light is polarized 45° to the *a*-axis of the sample. And its probe polarization dependence would exhibit the symmetry with period of π.

Reference

1. K. Persson, *Materials Data on $MnPS_3$ (SG:12) by Materials Project* (2016).
2. X.-C. Zhang and J. Xu, *Introduction to THz wave photonics* (Springer, 2010), Vol. 29.
3. L. D. Landau, J. S. Bell, M. J. Kearsley, L. P. Pitaevskii, E. M. Lifshitz, and J. B. Sykes, *Electrodynamics of Continuous Media* (Elsevier Science, 2013).